Second-harmonic generation in nanostructured metamaterials

Ulises R. Meza and Bernardo S. Mendoza
Department of Photonics, Centro de Investigaciones en Óptica, León, 37150 Guanajuato, México

W. Luis Mochán*
Instituto de Ciencias Físicas, Universidad Nacional Autónoma de México, Apartado Postal 48-3, 62251 Cuernavaca, Morelos, México

(Received 14 December 2018; revised manuscript received 16 February 2019; published 6 March 2019)

We conduct a theoretical and numerical study on the second-harmonic (SH) optical response of a nanostructured metamaterial composed of a periodic array of inclusions. Both the inclusions and their surrounding matrix are made of centrosymmetrical materials, for which SH is strongly suppressed, but, by appropriately choosing the shape of the inclusions, we may produce a geometrically noncentrosymmetric system which does allow efficient SH generation. Variations in the geometrical configuration allow tuning the linear and quadratic spectra of the optical response of the system. We develop a theory that allows the calculation of the nonlinear polarization from the geometry of the system and its linear dielectric function at the fundamental and second-harmonic frequencies, and we implement an efficient scheme for its numerical computation, extending a formalism for the calculation of the macroscopic dielectric function using Haydock's recursion method. We apply our formalism to an array of holes within an Ag matrix, but it can be readily applied to any metamaterial made of arbitrary materials and for inclusions of any geometry within the long-wavelength regime.

DOI: 10.1103/PhysRevB.99.125408

I. INTRODUCTION

The advent of structured metamaterials has allowed the design of new materials, with an unprecedented amount of control over their intrinsic properties. These metamaterials are typically composite systems that consist of two or more ordinary materials, that are periodically structured or arranged in such a manner that the resulting properties differ from those of the constituent materials. These systems have been widely explored both theoretically and experimentally, with a plethora of new applications under development [1–6]. The variety of available fabrication techniques such as electron-beam lithography [7–9], ion milling [10,11], and even conventional three-dimensional (3D) printing [12–14], allow for extremely precise designs of structured systems featuring arrays of inclusions (or holes) with specific shapes. These methods allow the fabrication of new devices with highly tunable optoelectronic properties [3,15]. A wide variety of applications using metamaterials have now been developed. Materials can be designed to have a negative index of refraction [16]. This has been implemented using periodic noble metal inclusions within a dielectric matrix [17]. Flat lens-like devices can be fabricated using metamaterials that can manipulate the propagation of light with subwavelength focusing capabilities [15]. This type of device has been implemented for cloaking [18–20] and shielding applications [21]. The fabrication of these materials is not restricted to specific ranges of the electromagnetic spectrum, permitting, for example, the development of new devices designed to work in the terahertz regime [22–24].

Metamaterials display a wide variety of optical phenomena [25]. Of particular interest to us are their nonlinear optical properties. The nonlinear response is strongly sensitive to the natural atomic structure. For second-harmonic generation (SHG) a material must have a noncentrosymmetric crystalline structure in order to have a strong dipolar nonlinear response. Structured metamaterials can be designed with almost limitless configurations and make for a promising alternative for nonlinear optical applications [26]. There have been numerous theoretical [6,27,28] and experimental [5,21,29] studies concerning the development of nonlinear devices using metamaterials. Some examples of nonlinear metamaterials have been fabricated using split-ring resonators [30,31] and nano-rod inclusions [32], producing SHG-active, magnetic, and left-handed materials. Other inclusions can be intrinsically noncentrosymmetric [33], thus creating a strong SHG response. Tailored metamaterials allow tuning the nonlinear optical response [34–37] through changes of the geometrical configuration. Plasmonic metamaterials may further enhance the nonlinearities through the field amplification associated to plasmonic resonances [38]. These systems can be varied geometrically, changing their degree of noncentrosymmetry, thus allowing for the second-harmonic (SH) signal to be even further enhanced.

An even richer set of possibilities opens up when 2D plasmonic metasurfaces are considered. These are made of arrays of structures with a subwavelength thickness known as *meta-atoms*, which permit the manipulation of the polarization, amplitude and phase of light. For example, a simple rotation of a noncentrosymmetric pseudo-atom allows a change of phase of the second harmonic field it generates, so that a metasurface whose atoms have a position dependent orientation may produce SHG beams propagating into specific angles according to its polarization. For a review of phenomena such as giant circular dichroism, nonlinear Berry phase and wavefront engineering and many others at nonlinear plasmonic metasurfaces

*mochan@fis.unam.mx

see Ref. [39]. Instead of plasmonic systems, for which dissipation may be problematic, all dielectric structures made of materials with a high index of refraction (high n) have also been proposed, where there are Mie-like resonances which yield large localized field amplitudes which produce nonlinear optical effects. Devices based on these resonances include controllable directional radiators due to the interference of electric and magnetic multipolar resonances, high efficiency metalenses, metasurface holograms and active nanophotonics [40,41]. It has been shown that in metasurfaces made of noncentrosymmetric high-n meta-molecules, made of pairs of slightly different meta-atoms, quasibound electromagnetic modes that coexist with the continuum of propagating electromagnetic waves may be excited, where the bound character arises due to the destructive interference between the far field of two modes whose frequencies display an avoided crossing as the geometric parameters of the system are varied. In this situation, the electric field in the neighborhood of the metamolecule is amplified, producing nonlinear effects, and, in particular, an orders-of-magnitude enhancement of the SHG [42].

The required physical parameters (namely, the electric permittivity and magnetic permeability) that are used for calculating the linear optical response can be obtained via a homogenization procedure [3,43,44]. The formalism presented in Refs. [45] and [46] is used in this work to describe the macroscopic linear response of inhomogeneous systems in terms of an average of certain specific microscopic response functions of the system. We first extend this formalism to calculate not only the linear but also the nonlinear optical second order susceptibility of metamaterials of arbitrary composition [47–51] in terms of its linear response and allowing for dispersion and dissipation. We illustrate the formalism exploring the nonlinear SH response of a periodic nanostructured 2D metamaterial comprised of an array of holes of a noncentrosymmetric shape within a matrix made of a centrosymmetric material, for which we chose silver. In this case, the SH generation from a homogeneous matrix would be strongly suppressed, but the noncentrosymmetric geometry of the holes allows a strong signal whose resonances may be tuned and enhanced through variations of the geometrical parameters [52,53]. We systematically study the evolution of the nonlinear susceptibility tensor due to variations in the shape and position of the holes. Last, we elucidate the origin of the produced SH response by calculating and analyzing the charge density and polarization field at the metallic surface. We have built computational packages for the calculation of the surface and bulk nonlinear polarization of nanostructured metamaterials and we have added them to the publicly available modular computational software PHOTONIC [54] developed by our group.

The paper is organized as follows. In Sec. II we present the theoretical approach used to calculate the dielectric response of the metamaterial that is then used to obtain the nonlinear SH polarization. In Sec. III we present results for a nanostructured metamaterial consisting of empty holes within a silver matrix. We explore a variety of geometric configurations to fine tune the SH response. Finally, in Sec. IV we present our conclusions.

II. THEORY

The quadratic polarization forced at the second-harmonic (SH) frequency 2ω by an inhomogeneous fundamental field $\boldsymbol{E}_\omega$ at frequency ω within an isotropic centrosymmetric material system made of polarizable entities within the nonretarded regime may be written as [55]

$$\boldsymbol{P}^f(2\omega) = n\boldsymbol{p}(2\omega) - \tfrac{1}{2}\nabla\cdot n\boldsymbol{Q}(2\omega), \tag{1}$$

where n is the number density of polarizable entities, $\boldsymbol{p}(2\omega)$ is their electric dipole moment, given within the *dipolium* model [56] by

$$\boldsymbol{p}(2\omega) = -\frac{n}{2e}\alpha(\omega)\alpha(2\omega)\nabla E^2(\omega), \tag{2}$$

$\boldsymbol{Q}(2\omega)$ is their electric quadrupole moment, given by

$$\boldsymbol{Q}(2\omega) = \frac{1}{2e}n\alpha^2(\omega)\boldsymbol{E}(\omega)\boldsymbol{E}(\omega), \tag{3}$$

and $\alpha(\nu\omega)$ are the the linear polarizabilities of each entity at the fundamental ($\nu = 1$) and at the SH ($\nu = 2$), related to the dielectric function $\epsilon(\nu\omega)$ through

$$\epsilon(\nu\omega) = 1 + 4\pi n\alpha(\nu\omega). \tag{4}$$

The nonlinear current density may be obtained from the polarization through $\boldsymbol{j}^f = \partial\boldsymbol{P}^f/\partial t$. We could expect an additional contribution $c\nabla\times\boldsymbol{M}^f$ from a magnetization $\boldsymbol{M}^f = n\boldsymbol{m}$, with $\boldsymbol{m}$ the second-order magnetic dipole moment of each polarizable entity. However, within the dipolium model the quadratic magnetic dipole induced in each polarizable entity is null for SHG [57–59].

We allow the density n, the polarizability α, the dielectric response ϵ, and the field to depend on position. The total polarization induced at the SH is then

$$\begin{aligned}\boldsymbol{P}(2\omega) &= n\alpha(2\omega)\boldsymbol{E}(2\omega) + \boldsymbol{P}^f(2\omega)\\ &= n\alpha(2\omega)\boldsymbol{E}(2\omega) - \frac{n}{2e}\alpha(\omega)\alpha(2\omega)\nabla E^2(\omega)\\ &\quad + \frac{1}{2e}\nabla\cdot n\alpha^2(\omega)\boldsymbol{E}(\omega)\boldsymbol{E}(\omega),\end{aligned} \tag{5}$$

where we added to Eq. (1) the polarization linearly induced by the self-consistent electric field $\boldsymbol{E}(2\omega)$ produced by the total SH polarization $\boldsymbol{P}(2\omega)$.

The equations above were developed for an insulating material, for which the polarizable entities are atoms whose electronic dynamics are described by harmonic forces, but by writing the linear polarizability at the fundamental and second-harmonic frequencies in terms of the dielectric function of the material, they can be applied to arbitrary insulators or semiconductors. An alternative model for the description of metals starts from the Euler hydrodynamic equation for their conduction electrons,

$$nm\left(\frac{\partial}{\partial t}\boldsymbol{v} + \boldsymbol{v}\cdot\nabla\boldsymbol{v} + \frac{\boldsymbol{v}}{\tau}\right) = -en\boldsymbol{E} - ne\frac{\boldsymbol{v}}{c}\times\boldsymbol{B}, \tag{6}$$

where n, $\boldsymbol{v}$, and τ are the electronic density, velocity, and lifetime respectively, and in which the nonlinearity arises from the magnetic interaction and the convective contribution to the time derivative. It has been shown that this model yields

the same result as the dipolium model when we identify $\boldsymbol{j} = -ne\boldsymbol{v}$ with the time derivative of the polarization $\boldsymbol{j} = \partial \boldsymbol{P}/\partial t$ and write the resulting response in terms of the linear dielectric function [57]. Thus, Eq. (5) describes the contributions of both bound and free electrons to the nonlinear polarization and can be used for metallic as well as dielectric systems.

We want to apply the equations above to obtain the nonlinear susceptibility of a binary metamaterial consisting of two phases: a host made up some material A in which inclusions made up of a material B are embedded forming a periodic lattice. In our actual calculations we will replace material B by vacuum. We denote by ϵ_γ, α_γ, and n_γ the dielectric function, polarizability and number density corresponding to material $\gamma = A,\ B$. We may describe the geometry of the metamaterial through a periodic *characteristic function* $B(\boldsymbol{r}) = B(\boldsymbol{r} + \boldsymbol{R})$ which takes the values 1 or 0, according to whether the position $\boldsymbol{r}$ lies within the region occupied by material B or A, respectively, and where $\boldsymbol{R}$ is a lattice vector. Thus, we may write the dielectric function as

$$\epsilon(\boldsymbol{r}) = \frac{\epsilon_A}{u}[u - B(\boldsymbol{r})], \tag{7}$$

where we introduced the spectral variable

$$u = \frac{1}{1 - \epsilon_B/\epsilon_A}, \tag{8}$$

which takes complex values in general and accounts for the composition of the materials and for their frequency-dependent response.

In the long-wavelength approximation, assuming that the unit cell of the metamaterial is small compared to the wavelength of light in vacuum and the wavelength or decay length within each of its components, the spatial fluctuations of the electric field are longitudinal [45] and the transverse or longitudinal nature of the macroscopic field is irrelevant, so we may take the electric field within a single cell as longitudinal $\boldsymbol{E} = \boldsymbol{E}^L$ and we may identify the longitudinal part $\boldsymbol{D}^L$ of the displacement field $\boldsymbol{D}$ as an *external* field, which therefore has no fluctuations originating in the spatial texture of the metamaterial, and is thus a macroscopic field $\boldsymbol{D}^L = \boldsymbol{D}^L_M$. Then, if we excite the system with a longitudinal external field, we may write

$$\boldsymbol{E} = (\hat{\boldsymbol{\epsilon}}^{LL})^{-1}\boldsymbol{D}^L \tag{9}$$

and

$$\boldsymbol{E}_M = \left(\hat{\boldsymbol{\epsilon}}^{LL}_M\right)^{-1}\boldsymbol{D}^L_M, \tag{10}$$

where $\hat{\boldsymbol{\epsilon}}^{LL} = \hat{\mathcal{P}}^L\hat{\epsilon}\hat{\mathcal{P}}^L$ is the longitudinal projection of the dielectric function ϵ interpreted as a linear operator;

$$\left(\hat{\boldsymbol{\epsilon}}^{LL}_M\right)^{-1} = \langle(\hat{\boldsymbol{\epsilon}}^{LL})^{-1}\rangle \tag{11}$$

is the inverse of the macroscopic longitudinal dielectric operator, given by the spatial average [45,46] $\langle\cdots\rangle$, of the *microscopic* inverse longitudinal dielectric operator; and $\hat{\mathcal{P}}^L$ is the longitudinal projector operator, which may be represented in reciprocal space by the matrix

$$\mathcal{P}_{\boldsymbol{G}\boldsymbol{G}'} = \hat{\boldsymbol{G}}\hat{\boldsymbol{G}}\delta_{\boldsymbol{G}\boldsymbol{G}'}, \tag{12}$$

where $\boldsymbol{G}$ and $\boldsymbol{G}'$ are reciprocal vectors of the metamaterial, $\delta_{\boldsymbol{G}\boldsymbol{G}'}$ is Kronecker's delta,

$$\hat{\boldsymbol{G}} = \frac{\boldsymbol{k} + \boldsymbol{G}}{||\boldsymbol{k} + \boldsymbol{G}||} \tag{13}$$

is a unit vector in the direction of the wave vector $\boldsymbol{k} + \boldsymbol{G}$, and $\boldsymbol{k}$ the conserved Bloch's vector of the linear field which we interpret as the relatively small wave vector of the macroscopic field.

From Eq. (7) we may write

$$(\hat{\boldsymbol{\epsilon}}^{LL})^{-1} = \frac{u}{\epsilon_A}(u\hat{\mathcal{P}}^L - \hat{B}^{LL})^{-1}, \tag{14}$$

in which we may interpret the inverse of the operator within parentheses in terms of a Green's function

$$\hat{\mathcal{G}}(u) = (u - \hat{\mathcal{H}})^{-1}, \tag{15}$$

the resolvent of a Hermitian operator $\hat{\mathcal{H}}$ with matrix elements

$$\mathcal{H}_{\boldsymbol{G}\boldsymbol{G}'} = \hat{\boldsymbol{G}} \cdot B(\boldsymbol{G} - \boldsymbol{G}')\hat{\boldsymbol{G}}' \tag{16}$$

in reciprocal space, where $B(\boldsymbol{G} - \boldsymbol{G}')$ is the Fourier coefficient of the periodic characteristic function $B(\boldsymbol{r})$ with wave vector $(\boldsymbol{G} - \boldsymbol{G}')$. Notice that $B^{LL}_{\boldsymbol{G}\boldsymbol{G}'} = \hat{\boldsymbol{G}}\mathcal{H}_{\boldsymbol{G}\boldsymbol{G}'}\hat{\boldsymbol{G}}'$, $(\boldsymbol{\epsilon}^{LL})^{-1}_{\boldsymbol{G}\boldsymbol{G}'} = (u/\epsilon_A)\hat{\boldsymbol{G}}\hat{\mathcal{G}}(u)\hat{\boldsymbol{G}}'$, and $(\boldsymbol{\epsilon}^{LL}_M)^{-1} = (u/\epsilon_A)\hat{\boldsymbol{k}}\langle\hat{\mathcal{G}}(u)\rangle\hat{\boldsymbol{k}}$.

To obtain the macroscopic dielectric response and the microscopic electric field we proceed as follows. We define a normalized macroscopic state $|0\rangle$ that represents a longitudinal field propagating with the given small wave vector $\boldsymbol{k}$, and we act repeatedly on this state with the operator $\hat{\mathcal{H}}$ to generate an orthonormal basis set $\{|n\rangle\}$ through Haydock's [60] recursion

$$\hat{\mathcal{H}}|n\rangle = b_{n+1}|n+1\rangle + a_n|n\rangle + b_n|n-1\rangle. \tag{17}$$

In this basis, $\hat{\mathcal{H}}$ may be represented by a tridiagonal matrix with elements

$$(\mathcal{H}_{nn'}) = \begin{pmatrix} a_0 & b_1 & 0 & 0 & \cdots \\ b_1 & a_1 & b_2 & 0 & \cdots \\ 0 & b_2 & a_2 & b_3 & \cdots \\ 0 & 0 & b_3 & a_3 & \cdots \\ \vdots & \vdots & \vdots & \vdots & \ddots \end{pmatrix} \tag{18}$$

given by Haydock's coefficients a_n and b_n. Thus, the macroscopic inverse longitudinal response may be obtained as a continued fraction [48,49]

$$\begin{aligned}\left(\boldsymbol{\epsilon}^{LL}_M\right)^{-1} &= \hat{\boldsymbol{k}}\hat{\boldsymbol{k}}\frac{u}{\epsilon_A}\langle 0|(u - \hat{H})^{-1}|0\rangle \\ &= \hat{\boldsymbol{k}}\hat{\boldsymbol{k}}\frac{u}{\epsilon_A}\cfrac{1}{u - a_0 - \cfrac{b_1^2}{u - a_1 - \cfrac{b_2^2}{u - a_2 - \cfrac{b_3^2}{\ddots}}}}\end{aligned} \tag{19}$$

and the microscopic electric field (9) may be represented in reciprocal space by

$$E_G = \sum \zeta_n\langle \boldsymbol{G}|n\rangle \tag{20}$$

with coefficients ζ_n obtained by solving the tridiagonal system

$$\sum_{n'}(u\delta_{nn'} - H_{nn'})\zeta_{n'} = \delta_{n0}D^L, \tag{21}$$

where we write the fields in real space as

$$\boldsymbol{D}^L(\boldsymbol{r}) = \hat{\boldsymbol{k}}D^L e^{i\boldsymbol{k}\cdot\boldsymbol{r}} \tag{22}$$

and

$$\boldsymbol{E}(\boldsymbol{r}) = \sum_{\boldsymbol{G}} \hat{\boldsymbol{G}}E_G e^{i(\boldsymbol{k}+\boldsymbol{G})\cdot\boldsymbol{r}}. \tag{23}$$

Notice that the results of the calculation above depend on the direction $\hat{\boldsymbol{k}}$ chosen as the propagation direction of the external field. As we may identify

$$\left(\boldsymbol{\epsilon}_M^{LL}\right)^{-1} = \frac{\hat{\boldsymbol{k}}\hat{\boldsymbol{k}}}{\hat{\boldsymbol{k}}\cdot\boldsymbol{\epsilon}_M\cdot\hat{\boldsymbol{k}}}, \tag{24}$$

all the components of the macroscopic dielectric tensor may be efficiently obtained from Eq. (19) by repeating the calculation of its longitudinal projection for different propagation directions $\hat{\boldsymbol{k}}$, such as along all independent combinations $\hat{\boldsymbol{e}}_i + \hat{\boldsymbol{e}}_j$ of pairs of Cartesian directions $\hat{\boldsymbol{e}}_i$ and $\hat{\boldsymbol{e}}_j$ ($i, j = x, y$, or z).

We remark that the small-scale fluctuations of the electric field within a nanostructured system within the long-wavelength regime *are* mostly longitudinal, as the transverse contributions are of an order a^2/λ^2 smaller [45,46], where a is the lattice parameter and λ the free-space wavelength. On the other hand, the macroscopic field is almost constant within the small unit cell, so its transverse or longitudinal character is irrelevant. For these reasons, after having identified all of the components of the dielectric tensor, the results above are suitable for the common case of electromagnetic waves for which the macroscopic field is actually transverse, not longitudinal. These remarks have been verified by comparing the full numerical solution of the wave equation within a metamaterial with the efficient solution proposed above [47,61].

Once we obtain the microscopic field from Eqs. (20), (21), and (23), we may substitute it in Eqs. (1)–(3) to obtain the forced SH polarization, which we may then substitute in Eq. (5) to obtain the self-consistent quadratic polarization in the SH. However, in order to solve Eq. (5) we need the self-consistent SH field, which in the long-wavelength approximation is simply given by the depolarization field

$$\boldsymbol{E}(2\omega) = -4\pi\boldsymbol{P}^L(2\omega) \tag{25}$$

produced only by the longitudinal part of the SH polarization. Thus we write Eq. (5) as

$$\boldsymbol{P}(2\omega) = -4\pi n\alpha(2\omega)\boldsymbol{P}^L(2\omega) + \boldsymbol{P}^f(2\omega). \tag{26}$$

By taking its longitudinal projection, we obtain a closed equation for $\boldsymbol{P}^L(2\omega)$ which we solve formally as

$$\boldsymbol{P}^L(2\omega) = (\hat{\boldsymbol{\epsilon}}^{LL}(2\omega))^{-1}\boldsymbol{P}^{fL}(2\omega) \tag{27}$$

using Eq. (4). Plugging this result back into Eq. (26), we finally obtain the SH polarization $\boldsymbol{P}(2\omega)$.

In order to perform the operation indicated in Eq. (27) we perform a Haydock recursion as in Eq. (17) but using

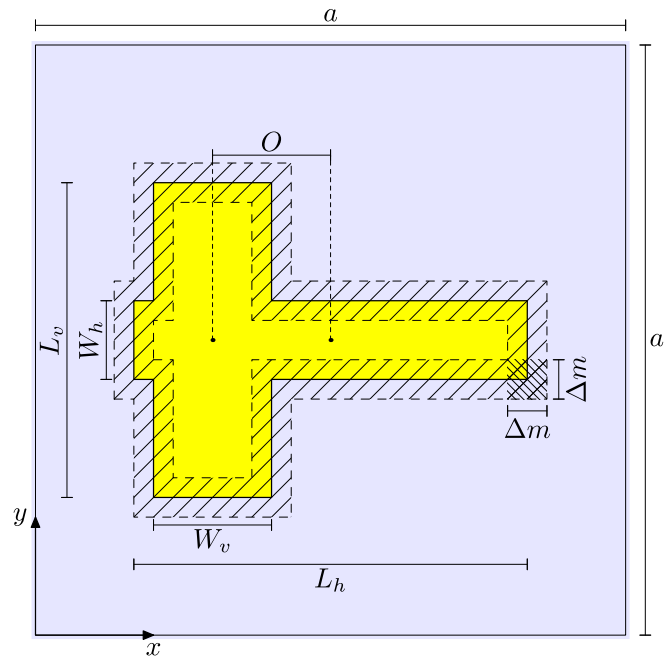

FIG. 1. Unit cell of a metamaterial made up of a horizontal and a vertical rectangular hole within a conducting matrix. We indicate the lattice parameter a of the square array, the length L_β and width W_β of each rectangle ($\beta = h, v$), and the offset O of the center of the vertical rectangle with respect to that of the horizontal one. We indicate the directions x, y of the crystalline axes. The shaded regions correspond to masks of width Δm used to single out the surface, edge, and corner contributions to the SH response.

$\boldsymbol{P}^{fL}(2\omega)$ to construct a new initial normalized state $|\tilde{0}\rangle$, with components $\langle\boldsymbol{G}|\tilde{0}\rangle$ in reciprocal space given by

$$\boldsymbol{P}_{\boldsymbol{G}}^{fL}(2\omega) = \hat{\boldsymbol{G}}\langle\boldsymbol{G}|\tilde{0}\rangle f, \tag{28}$$

where f is a normalization constant. From this state, we build a new Haydock orthonormal basis $|\tilde{n}\rangle$ using the same procedure as in Eq. (17). Thus, we write the self-consistent longitudinal SH polarization as

$$\boldsymbol{P}^L(2\omega;\boldsymbol{r}) = \sum_{\boldsymbol{G}} P_{\boldsymbol{G}}^L(2\omega)\hat{\boldsymbol{G}}e^{i(\boldsymbol{k}+\boldsymbol{G})\cdot\boldsymbol{r}}, \tag{29}$$

with

$$P_{\boldsymbol{G}}^L(2\omega) = \frac{u_2}{\epsilon_{A2}}\sum_{\tilde{n}}\xi_{\tilde{n}}\langle\boldsymbol{G}|\tilde{n}\rangle \tag{30}$$

and with coefficients $\xi_{\tilde{n}}$ obtained by solving the tridiagonal system

$$\sum_{\tilde{n}'}(u_2\delta_{\tilde{n}\tilde{n}'} - H_{\tilde{n}\tilde{n}'})\xi_{\tilde{n}'} = \delta_{\tilde{n}\tilde{0}}f, \tag{31}$$

where u_2 and ϵ_{A2} are the spectral variable (8) and the dielectric response ϵ_A but evaluated at the SH frequency 2ω.

Substitution of $\xi_{\tilde{n}}$ from Eq. (31) into Eqs. (30) and (29) yields the SH longitudinal polarization, which may then be substituted into Eq. (26) to obtain the total SH polarization in the long-wavelength limit when the system is excited by a longitudinal external field along $\hat{\boldsymbol{k}}$. Averaging the result, or equivalently taking the $\boldsymbol{G} = 0$ contribution in reciprocal

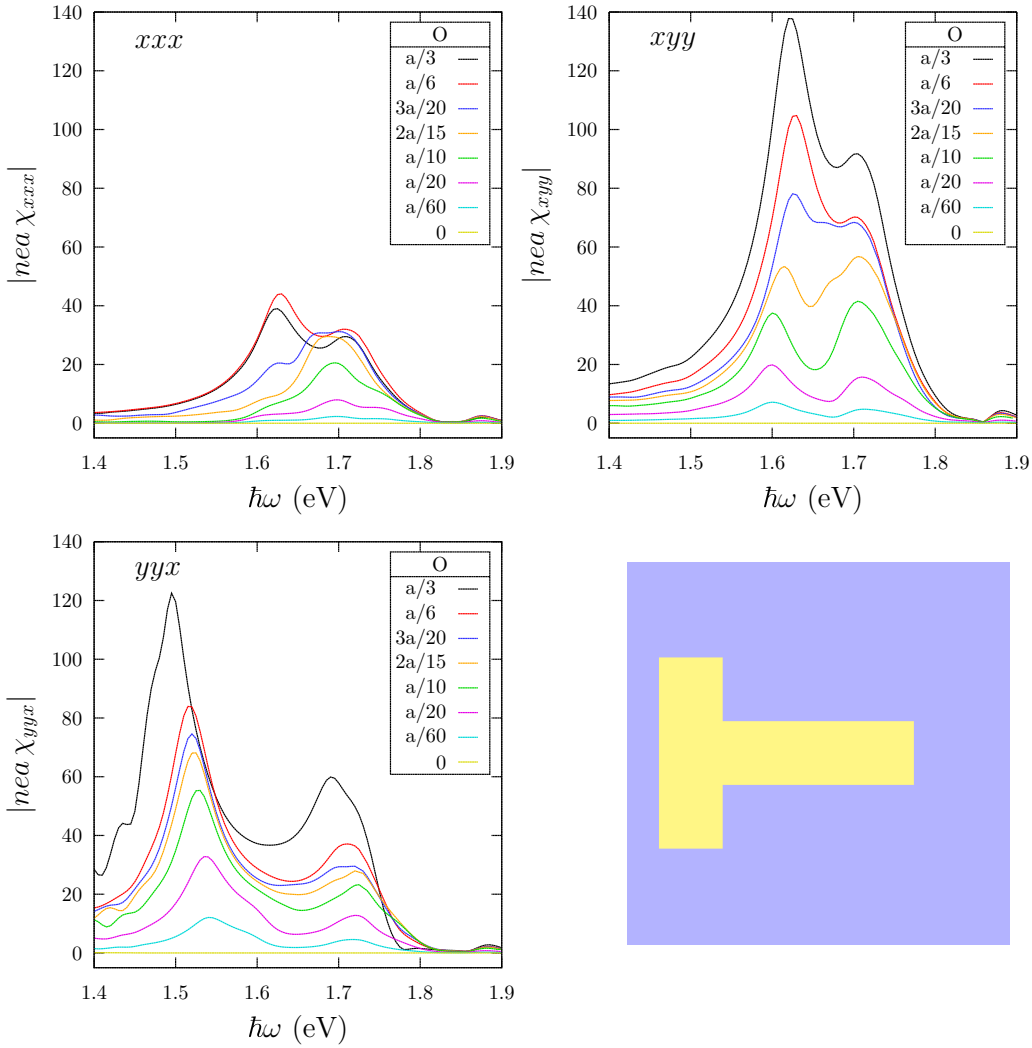

FIG. 2. Normalized absolute value of the non-null components of the SH susceptibility $nea\chi_{ijk}$, with $ijk = xxx$ (upper left), xyy (upper right), and $yyx = yxy$ (lower left), for a square lattice of rectangular holes, as in Fig. 1 within an Ag matrix, with geometrical parameters $L_h = L_v = a/2$, $W_h = W_v = a/6$, for different values of the offset $O = 0, \ldots, a/3$. The lower right panel displays the geometry corresponding to the largest offset. Notice that for these cases the holes overlap.

space, we obtain the macroscopic SH polarization $\boldsymbol{P}_M(2\omega)$. Notice that we may *not* obtain yet the nonlinear quadratic susceptibility from this polarization, as it contains a contribution from the linear response to the second harmonic electric field. Thus, we write

$$\boldsymbol{P}_M(2\omega) = \frac{1}{4\pi}(\boldsymbol{\epsilon}_M(2\omega) - \mathbf{1})\boldsymbol{E}_M(2\omega) + \boldsymbol{P}_M^f(2\omega), \qquad (32)$$

where the first term is the contribution of the linear response at 2ω to the SH macroscopic field, and the second term

$$\boldsymbol{P}_M^f(2\omega) = \boldsymbol{\chi}_M^{(2)} : \boldsymbol{E}_M(\omega)\boldsymbol{E}_M(\omega) \qquad (33)$$

is the sought after contribution to the SH macroscopic polarization forced by the fundamental macroscopic electric field, and $\boldsymbol{\chi}_M^{(2)}$ is the corresponding SH quadratic macroscopic susceptibility, given by a third-rank tensor. Within our long-wavelength longitudinal calculation the macroscopic field $\boldsymbol{E}_M(2\omega)$ is simply given by the longitudinal depolarization field

$$\boldsymbol{E}_M(2\omega) = \boldsymbol{E}_M^L(2\omega) = -4\pi\boldsymbol{P}_M^L(2\omega), \qquad (34)$$

so that, taking the longitudinal projection of Eq. (32), we obtain

$$\boldsymbol{P}_M^{fL}(2\omega) = \hat{\boldsymbol{k}}\hat{\boldsymbol{k}} \cdot \boldsymbol{P}_M^f(2\omega) = \boldsymbol{\epsilon}_M^{LL}(2\omega)\boldsymbol{P}_M^L(2\omega). \qquad (35)$$

Substituting $\boldsymbol{P}_M^{fL}(2\omega)$ from Eq. (35) into (34) and then into (32) we obtain the macroscopic forced quadratic SH polarization $\boldsymbol{P}_M^f(2\omega)$ produced by a longitudinal external $\boldsymbol{D}^L$ field pointing along $\hat{\boldsymbol{k}}$. As in the linear case, we finally repeat the calculation above, for several independent directions of propagation $\hat{\boldsymbol{k}}$ so that Eq. (33) becomes a system of linear equations in the unknown Cartesian components $\chi_{M\,ijk}^{(2)}$ ($i, j, k = x$, y, or z), which we solve to obtain the third-rank second-order susceptibility tensor $\boldsymbol{\chi}_M^{(2)}$ of the metamaterial. Notice that a quadratic macroscopic electric quadrupolar density, as well as a possible quadratic macroscopic magnetic dipolar density, could also produce a nonlocal contribution to

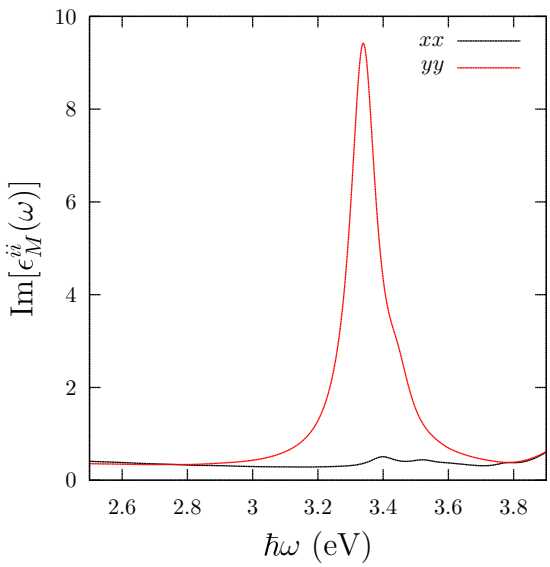

FIG. 3. Non-null components of the macroscopic dielectric response, ϵ_M^{xx} and ϵ_M^{yy}, of a metamaterial made up of a square array of horizontally oriented single rectangular holes with the same dimensions as in Fig. 2 within an Ag matrix.

the polarization, described by a fourth-order tensor which acts on $\boldsymbol{E}_M\nabla\boldsymbol{E}_M$. This terms would be negligible within the long-wavelength regime, except for centrosymmetric systems with a centrosymmetric geometry, for which the local contribution is suppressed.

In summary, to obtain the quadratic response we first obtain the nonretarded microscopic field and the macroscopic dielectric tensor using a Haydock's recursion starting from a macroscopic external longitudinal field; then we use the dipolium model to obtain the microscopic *source* of the SH polarization, and we screen it using Haydock's scheme again to obtain the *full* microscopic polarization, which we average to obtain the full macroscopic SH polarization. As this *includes* a contribution from the *macroscopic SH depolarization field*, we subtract it before identifying the quadratic susceptibility tensor projected onto the longitudinal direction. We repeat the calculation along different independent directions so that we can extract all the components of the quadratic susceptibility.

In the process above we assumed that the unit cell of the metamaterial is small with respect to the wavelength at frequency ω, and thus we introduced a long-wavelength approximation and assumed the external field and the electric field to be longitudinal. After obtaining all the components of the macroscopic response, we should not concern ourselves anymore with the texture of the metamaterial; the unit cell disappears from any further use we give to the macroscopic susceptibility. Thus, we can solve any macroscopic SH related electromagnetic problem using the susceptibility obtained above without using again the long-wavelength approximation. Once we have the full macroscopic susceptibility tensor we may use it to calculate the response *to transverse* as well as longitudinal fields. Thus, we may use our susceptibility above to study the generation of electromagnetic waves at the SH from a propagating fundamental wave, in which case the macroscopic fields *can no longer* be assumed to be longitudinal; it is only their spatial fluctuations, which have been homogenized away, that are necessarily longitudinal.

III. RESULTS

In the present section we apply the formalism developed in the previous section to obtain the nonlinear response of a system with a simple geometry for which we can control the degree of centrosymmetry. To that end, we incorporated the scheme described in the previous section into the publicly

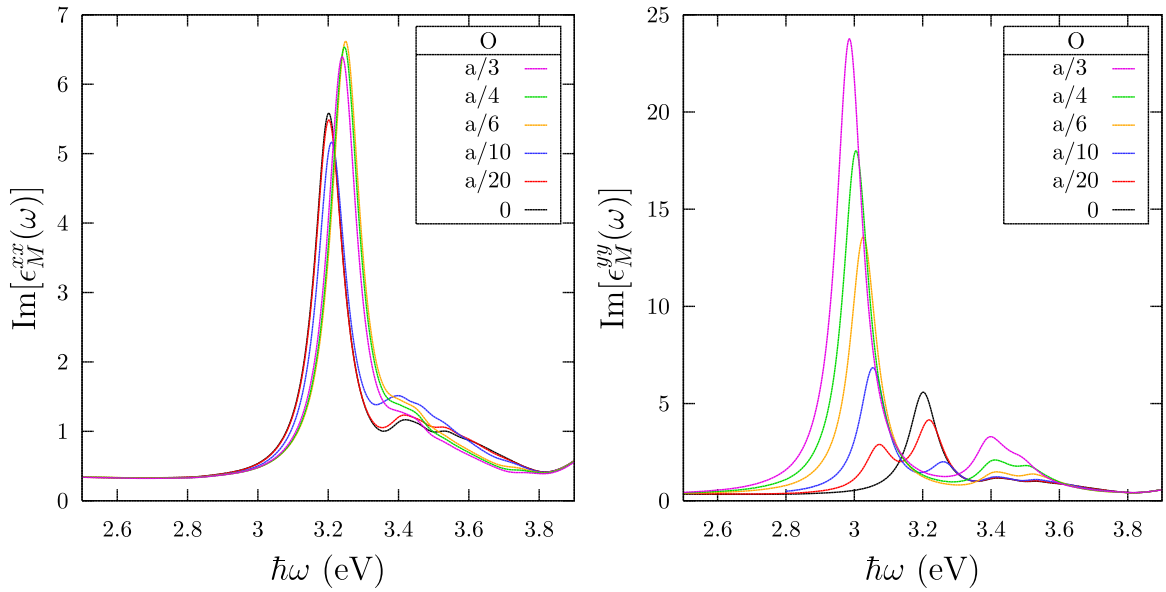

FIG. 4. Non-null components ϵ_M^{xx} and ϵ_M^{yy} of the macroscopic dielectric tensor $\boldsymbol{\epsilon}_M$ of a metamaterial made up of a square lattice of pairs of horizontally and vertically oriented single rectangular holes within an Ag matrix as in Fig. 1 with the same parameters as in Fig. 2 for different values of the offset $O = 0, \ldots, a/3$.

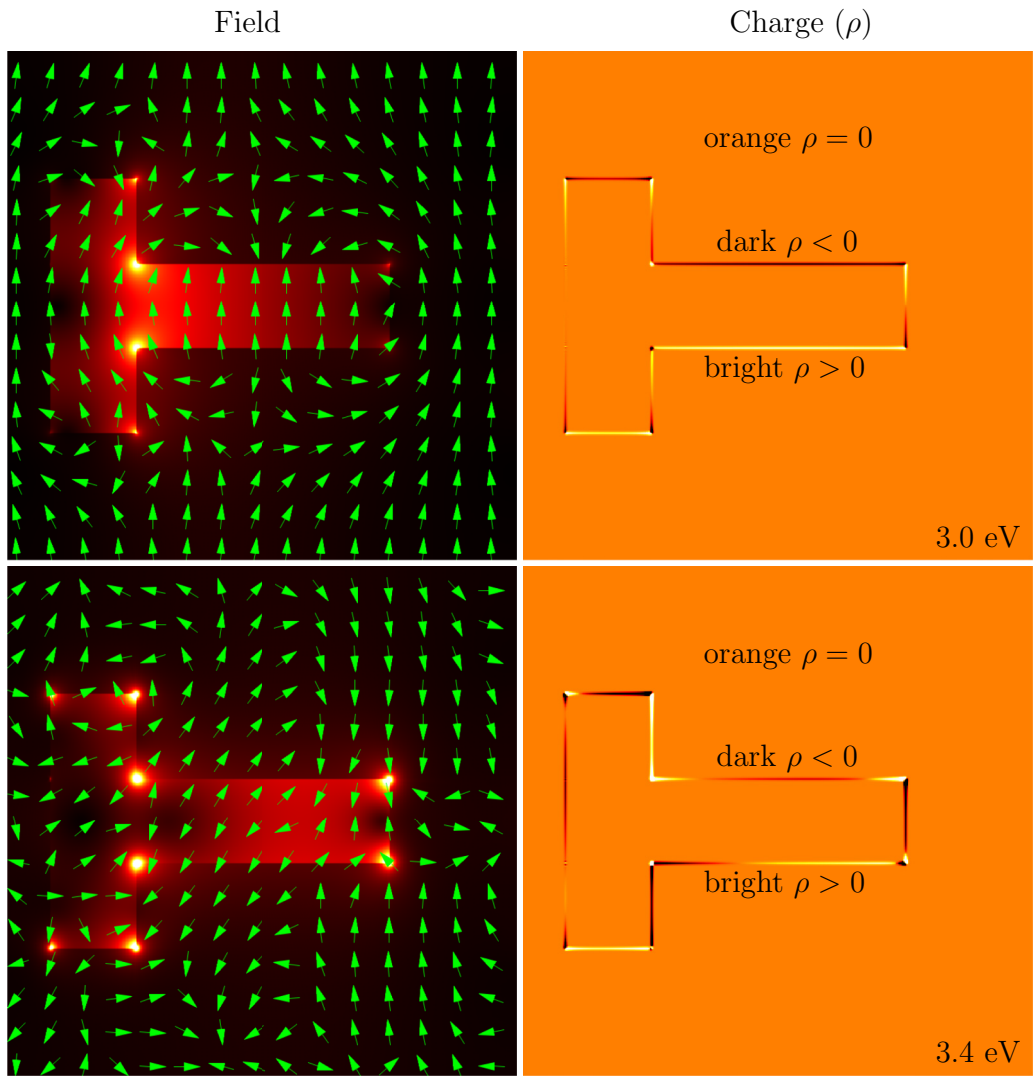

FIG. 5. Magnitude (color coded) and direction (arrows) of the microscopic linear electric field (left) and induced charge density ρ (right) for a metamaterial made of a square lattice of rectangular holes within an Ag matrix with the same parameters as in Fig. 2 with an offset $O = a/3$, excited by a macroscopic field along the y (vertical) direction for $\hbar\omega \approx 3\,\mathrm{eV}$ and $\hbar\omega \approx 3.4\,\mathrm{eV}$ corresponding to the two peaks in ϵ_M^{yy} shown in Fig. 4. The field and the charge distribution correspond to a vertical polarization for the horizontal rectangle, a vertical polarization for the vertical rectangle, and a nondiagonal quadrupole with opposite horizontal polarizations above and below the symmetry plane.

available package PHOTONIC [54], which is a modular, object-oriented system based on the Perl programming language, its Perl Data Language (PDL) [62] extension for efficient numerical calculations, and the Moose [63] object system. The package implements Haydock's recursive procedure to calculate optical properties of structured metamaterials in the nonretarded as well as in the retarded regime.

Our system consists of a square array of pairs of holes in the shape of prisms with a rectangular cross section within a metallic host (Fig. 1). Each rectangle is aligned with one of the crystalline axes x, y of the metamaterial and is characterized by its length L_h or L_v and its width W_h or W_v, where h denotes horizontal (along x) and v vertical (along y) alignment. The center of the vertical rectangle is shifted horizontally with respect to the center of the horizontal rectangle by an offset O. Thus, when $O = 0$ our system is centrosymmetric and as O increases it becomes noncentrosymmetric in varying degrees.

We remark that we have chosen an essentially 2D system, assuming full translational invariance along the third dimension, as this choice allows a full analysis of the ensuing results below. Nevertheless, our formalism may also be applied to periodical binary 1D and 3D systems [48]. Furthermore, we can generalize our results to systems with an arbitrary number of phases [64] and we can apply them to finite systems such as metasurfaces.

In order to simplify our analysis, we have chosen a system that has mirror symmetry $y \leftrightarrow -y$. Thus, the only in-plane non-null components of the SH susceptibility are [65] χ_{xxx}, χ_{xyy}, and $\chi_{yxy} = \chi_{yyx}$. We omit the subindex M and the superindex (2) that indicate these are components of the quadratic macroscopic susceptibility in order to simplify the notation, as we expect it yields no confusion. In Fig. 2 we show the spectra of the magnitude of these non-null components for an Ag host [66] and for different values of the offset

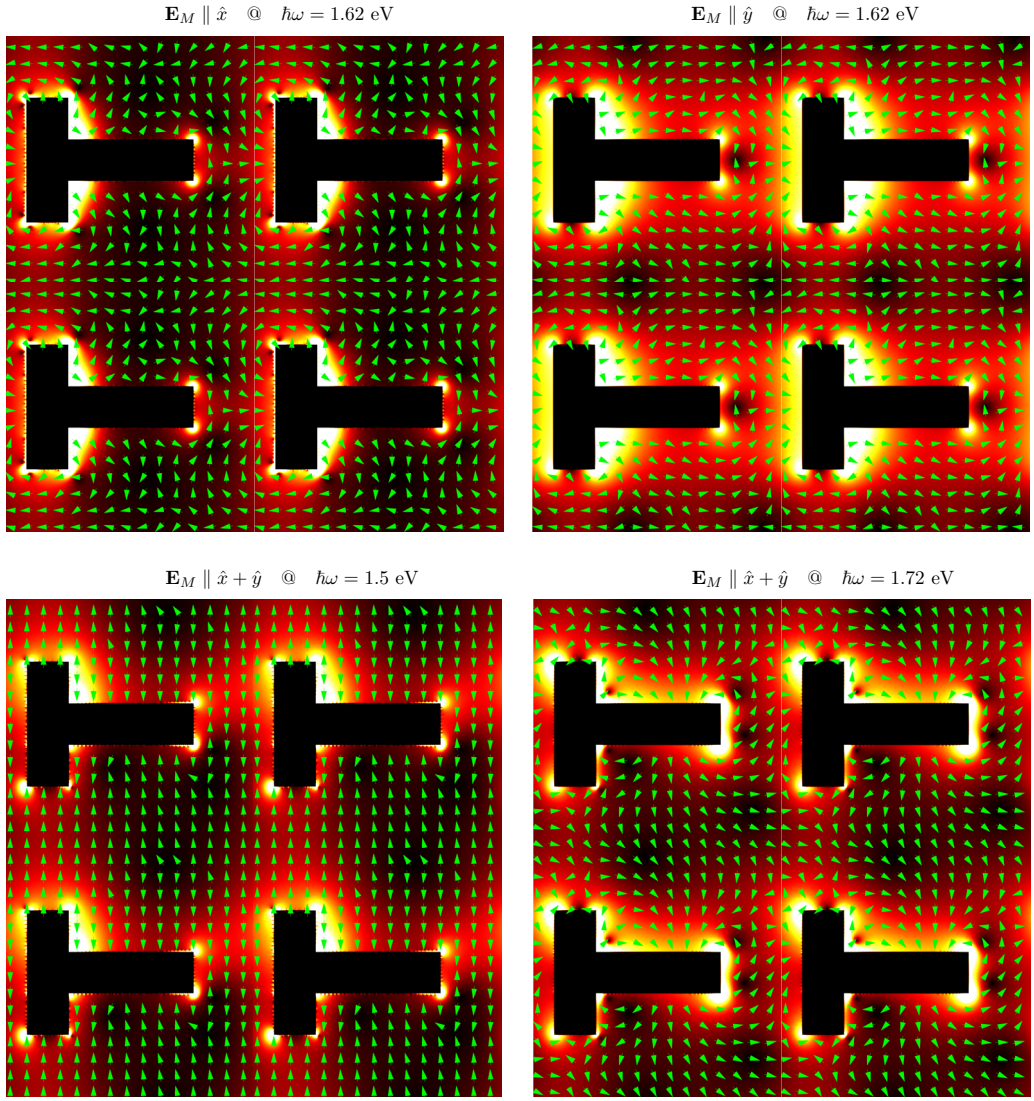

FIG. 6. Magnitude and direction of the quadratic polarization induced in the same system as in Fig. 2 for the largest offset $O = a/3$ at the resonant energy $\hbar\omega = 1.62$ eV and the fundamental macroscopic field $\boldsymbol{E}_M$ along the direction $\hat{x}$ (upper left), at $\hbar\omega = 1.62$ eV and $\boldsymbol{E}_M$ along y (upper right), and at $\hbar\omega = 1.5$ eV and $\hbar\omega = 1.72$ eV with $\boldsymbol{E}_M$ along $\hat{x} + \hat{y}$ (bottom).

O. The parameters we used were $W_h = W_v = a/6$, $L_h = L_v = a/2$, $O = 0, \ldots, a/3$. Notice that when $O = 0$ the system is centrosymmetric and there is no SH signal. As O increases towards $\pm a/3$ the system becomes noncentrosymmetric. Two resonances become clearly visible and they grow in size as O increases and the system moves farther away from the centrosymmetric case. The lower energy resonance of χ_{yyx} is at a different frequency than those of χ_{xxx} and χ_{xyy} and is redshifted as the offset increases. If O increases beyond $a/3$ (not shown) the two rectangles would cease to overlap and the quadratic susceptibility would rapidly decay, until $O = a/2$ for which the system becomes exactly centrosymmetric again and the quadratic susceptibility becomes exactly null.

According to Fig. 2, the order of magnitude of the SH susceptibility at resonance is around $10^2/nea$. For typical noncentrosymmetrical materials, such as quartz, AlGaAs or LiNbO3, the corresponding order of magnitude is around $1/nea_B$, where a_B is Bohr radius [67]. Thus, a centrosymmetric metallic material with a noncentrosymmetric geometry can achieve at resonance susceptibilities as large as $10^2 a_B/a$ times that of noncentrosymmetrical materials, even accounting for their large dissipation; for a unit cell of around 100 nm this would be just one order of magnitude below those of the above mentioned systems [68].

In order to understand the origin of the structure of the spectra discussed above, in Fig. 3 we plot the non-null components ϵ_M^{xx} and ϵ_M^{yy} of the macroscopic linear dielectric tensor $\boldsymbol{\epsilon}_M$ of a metamaterial made up of a square lattice of *single* rectangular holes with a horizontal orientation. Notice that there is a very weak resonance close to 3.4 eV corresponding to polarization along the length of the rectangle (x direction) and a strong resonance corresponding to polarization along the width of the rectangle (y direction) at a slightly smaller frequency. Although there is a strong linear resonance in the y direction, this system is centrosymmetrical and would yield no SH signal. When we combine horizontal and

vertical rectangles (Fig. 4) with a null offset $O = 0$ to make a centrosymmetric array of crosses, both resonances appear for both polarizations, although they now interact, partially exchange their strengths and repel so that both become clearly visible close to 3.4 and 3.2 eV.

As the offset O increases, there are only small changes to the spectra corresponding to ϵ_M^{xx}, consisting in changes to the weights of the peaks. However, a new strong mode develops in the spectra of ϵ_M^{yy}. This mode is due to the strong coupling of a quadrupolar oscillation in the vertical rectangle to the vertical dipolar oscillation of the horizontal rectangle. This quadrupole may be visualized as a horizontal polarization in the upper part of the vertical rectangle and a horizontal polarization in the opposite direction in the lower part of the rectangle, as illustrated by Fig. 5. The coupling is symmetry allowed as for a finite offset $O \neq 0$ the system looses the $x \leftrightarrow -x$ symmetry.

We expect the resonant structure of the quadratic susceptibility to have peaks corresponding to the resonances of the linear response at the fundamental and at the SH frequency. Thus, we expect peaks at the fundamental and at the subharmonics of those of the linear response. As there is no structure in the linear response within the region from 1.4 to 1.9 eV shown in Fig. 2, in our system we can only expect structure at the subharmonics, due to a resonant excitation of the polarization at the SH frequency. For a macroscopic field oriented along the Cartesian directions x or y the SH harmonic polarization can only point along the x direction, due to the $y \leftrightarrow -y$ mirror symmetry of our system. Thus, the subharmonics of the resonances of ϵ_M^{xx} (Fig. 4) appear in the susceptibility components χ_{xxx} and χ_{xyy} (Fig. 2). On the other hand, a macroscopic field that points along an intermediate direction between x and y may excite a quadratic polarization along y. Thus, the subharmonics of the resonances of ϵ_M^{yy} (Fig. 4) appear in the susceptibility components $\chi^{yxy} = \chi^{yyx}$ (Fig. 2).

To gain further insight into the nature of the resonances, in Fig. 6 we show the polarization maps evaluated at the maxima of the SH spectra corresponding to different directions of the macroscopic linear field, and for the offset $O = a/3$ that yields the largest signals. We notice that when the fundamental macroscopic field points along the x or along the y direction, the magnitude of the SH polarization is symmetric with respect to the mirror plane, and the y component of the polarization points towards opposite directions on either side of the mirror plane, yielding a macroscopic SH polarization along x. In these cases, the polarization has maxima near the four concave vertices of the vertical hole and near the convex vertex where the horizontal and vertical rectangles meet. On the other hand, when the fundamental macroscopic field points along the direction of $\hat{x} + \hat{y}$, the resulting quadratic polarization has no symmetry at all, and it yields a macroscopic SH polarization that has a y component.

Finally, in Fig. 7 we illustrate the contributions of the surface region to the total quadratic susceptibility by adding only the contributions within bands of varying widths Δm around the surface. We notice that although there is a very strong surface polarization, its contribution to the macroscopic quadratic susceptibility is relatively small, as it is confined to a very narrow region and it is partially canceled by the polarization at other parts of the surface, so that for the geometry studied here most of the SH signal comes from the bulk of the host.

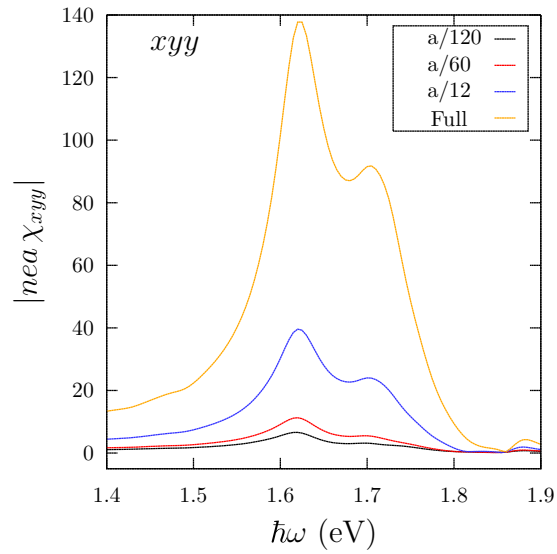

FIG. 7. Contributions to the quadratic susceptibility χ_{xyy} of the same system as in Fig. 6 from the region within a distance Δm from the surface, as defined in Fig. 1 for values of $\Delta m = a/120, a/60, a/12$, and the full susceptibility.

IV. CONCLUSIONS

We have developed a formalism for the calculation of the second-order susceptibility of structured binary metamaterials formed by a lattice of particles embedded within a host, for the case where both components consists of centrosymmetric materials but where the geometry is not centrosymmetric. Although SH is strongly suppressed within a homogeneous centrosymmetric material, the noncentrosymmetric surface is capable of sustaining a surface nonlinear polarization and inducing a strongly varying linear field which produces a multipolar nonlinear polarization within the metamaterial components.

We implemented our formalism using the Haydock recursive scheme within the freely available PHOTONIC modular package and applied it to the calculation of the second-order nonlinear susceptibility of a structured metamaterial composed of a homogeneous Ag host with a lattice of pairs of rectangular holes. Although the chosen system is 2D, the formalism may be applied as well to 1D or 3D systems and may be generalized to multicomponent finite systems such as metasurfaces. By modifying the geometry of the holes, we modify the degree of noncentrosymmetry of the material, allowing us to fine tune both the peak position and intensity of the SH response. The SH signal is very sensitive to changes in the geometrical parameters of the structure.

After establishing the inclusion shape that most enhances this signal, we analyzed the polarization field and showed that the SH response is largest at resonance close to the concave and convex corners but it extends well into the host material. The order of magnitude of the susceptibility obtained in this

calculation is comparable to that of typical noncentrosymmetric materials.

Although this study was carried out for one particular combination of materials, the employed procedure is equally valid for calculating the nonlinear properties for any metamaterial composed of arbitrary materials and inclusions. Only *a priori* knowledge of the dielectric function of each constituent material is required. This approach affords the opportunity to quickly and efficiently study a limitless range of possible metamaterial designs, with manifold optical applications in mind. Our hope is that this methodology will prove to be an important tool for future metamaterial design and fabrication.

ACKNOWLEDGMENTS

This work was supported by DGAPA-UNAM under Grants No. IN113016 and No. IN111119 (WLM) and by CONACyT under scholarship 589138 (U.R.M.). We acknowledge useful talks with Raksha Singla and Sean M. Anderson.

[1] V. Veselago, Usp. Phys. Sci. **92**, 517 (1967).
[2] J. C. Garland and D. B. Tanner, *Electrical Transport and Optical Properties of Inhomogeneous Media*, Technical Report (American Institute of Physics, New York, 1978).
[3] D. R. Smith, W. J. Padilla, D. C. Vier, S. C. Nemat-Nasser, and S. Schultz, Phys. Rev. Lett. **84**, 4184 (2000).
[4] D. R. Smith, J. B. Pendry, and M. C. K. Wiltshire, Science **305**, 788 (2004).
[5] H. Husu, R. Siikanen, J. Makitalo, J. Lehtolahti, J. Laukkanen, M. Kuittinen, and M. Kauranen, Nano Lett. **12**, 673 (2012).
[6] S. Larouche and D. R. Smith, Opt. Commun. **283**, 1621 (2010).
[7] Y. Akahane, T. Asano, B.-S. Song, and S. Noda, Nature (London) **425**, 944 (2003).
[8] A. Grigorenko, A. Geim, H. Gleeson, Y. Zhang, A. Firsov, I. Khrushchev, and J. Petrovic, Nature (London) **438**, 335 (2005).
[9] S. Balci, D. A. Czaplewski, I. W. Jung, J.-H. Kim, F. Hatami, P. Kung, and S. M. Kim, IEEE J. Sel. Top. Quantum Electron. **23**, 1 (2017).
[10] R. Gordon, A. G. Brolo, A. McKinnon, A. Rajora, B. Leathem, and K. L. Kavanagh, Phys. Rev. Lett. **92**, 037401 (2004).
[11] G. Seniutinas, A. Balčytis, Y. Nishijima, A. Nadzeyka, S. Bauerdick, and S. Juodkazis, Appl. Phys. A **122**, 383 (2016).
[12] M. Wegener, in *Laser Applications in Microelectronic and Optoelectronic Manufacturing (LAMOM) XXIII*, SPIE Proceedings Vol. 10519 (International Society for Optics and Photonics, Bellingham, WA, 2018), p. 1051910.
[13] Z. Shen, H. Yang, X. Huang, and Z. Yu, J. Opt. **19**, 115101 (2017).
[14] E. Mikheeva, R. Abdeddaim, S. Enoch, J. Wenger, F. Lemarchand, A. Moreau, I. Voznyuk, and J. Lumeau, in *Advances in Optical Thin Films VI*, SPIE Proceedings Vol. 10691 (International Society for Optics and Photonics, Bellingham, WA, 2018) p. 106911T.
[15] J. B. Pendry, Phys. Rev. Lett. **85**, 3966 (2000).
[16] V. M. Shalaev, W. Cai, U. K. Chettiar, H.-K. Yuan, A. K. Sarychev, V. P. Drachev, and A. V. Kildishev, Opt. Lett. **30**, 3356 (2005).
[17] A. V. Kildishev, W. Cai, U. K. Chettiar, H.-K. Yuan, A. K. Sarychev, V. P. Drachev, and V. M. Shalaev, J. Opt. Soc. Am. B **23**, 423 (2006).
[18] J. B. Pendry, D. Schurig, and D. R. Smith, Science **312**, 1780 (2006).
[19] U. Leonhardt, Science **312**, 1777 (2006).
[20] J. Hao, W. Yan, and M. Qiu, Appl. Phys. Lett. **96**, 101109 (2010).
[21] S. Feng and K. Halterman, Phys. Rev. Lett. **100**, 063901 (2008).
[22] L. V. Alekseyev, V. A. Podolskiy, and E. E. Narimanov, Adv. OptoElectron. **2012**, 267564 (2012).
[23] N. Born, R. Gente, I. Al-Naib, and M. Koch, Electron. Lett. **51**, 1012 (2015).
[24] T. Suzuki, M. Sekiya, T. Sato, and Y. Takebayashi, Opt. Express **26**, 8314 (2018).
[25] H. Chen, C. T. Chan, and P. Sheng, Nat. Mater. **9**, 387 (2010).
[26] M. Lapine, I. V. Shadrivov, and Y. S. Kivshar, Rev. Mod. Phys. **86**, 1093 (2014).
[27] K. O'Brien, H. Suchowski, J. Rho, A. Salandrino, B. Kante, X. Yin, and X. Zhang, Nat. Mater. **14**, 379 (2015).
[28] S. Larouche and V. Radisic, Phys. Rev. A **97**, 043863 (2018).
[29] I. V. Shadrivov, A. A. Zharov, and Y. S. Kivshar, J. Opt. Soc. Am. B **23**, 529 (2006).
[30] A. A. Zharov, I. V. Shadrivov, and Y. S. Kivshar, Phys. Rev. Lett. **91**, 037401 (2003).
[31] M. W. Klein, C. Enkrich, M. Wegener, and S. Linden, Science **313**, 502 (2006).
[32] G. Marino, P. Segovia, A. V. Krasavin, P. Ginzburg, N. Olivier, G. A. Wurtz, and A. V. Zayats, Laser Photonics Rev. **12**, 1700189 (2018).
[33] B. K. Canfield, H. Husu, J. Laukkanen, B. Bai, M. Kuittinen, J. Turunen, and M. Kauranen, Nano Lett. **7**, 1251 (2007).
[34] P.-Y. Chen, C. Argyropoulos, and A. Alù, Nanophotonics **1**, 221 (2012).
[35] D. Timbrell, J. W. You, Y. S. Kivshar, and N. C. Panoiu, Sci. Rep. **8**, 3586 (2018).
[36] J. Bar-David and U. Levy, in *CLEO: Science and Innovations* (Optical Society of America, Washington, 2018), pp. JW2A–98.
[37] M. Galanty, O. Shavit, A. Weissman, H. Aharon, D. Gachet, E. Segal, and A. Salomon, Light: Sci. Appl. **7**, 49 (2018).
[38] M. Kauranen and A. V. Zayats, Nat. Photonics **6**, 737 (2012).
[39] G. Li, S. Zhang, and T. Zentgraf, Nat. Rev. Mater. **2**, 17010 (2017).
[40] S. Kruk and Y. Kivshar, ACS Photonics **4**, 2638 (2017).
[41] Y. Kivshar, Natl. Sci. Rev. **5**, 144 (2018).
[42] K. Koshelev, A. Bogdanov, and Y. Kivshar, Science Bulletin, doi:10.1016/j.scib.2018.12.003.
[43] C. R. Simovski, J. Opt. **13**, 013001 (2010).
[44] A. Alu, Phys. Rev. B **84**, 075153 (2011).
[45] W. L. Mochán and R. G. Barrera, Phys. Rev. B **32**, 4984 (1985).
[46] W. L. Mochán and R. G. Barrera, Phys. Rev. B **32**, 4989 (1985).
[47] E. Cortes, L. Mochán, B. S. Mendoza, and G. P. Ortiz, Phys. Status Solidi B **247**, 2102 (2010).

[48] W. L. Mochán, G. P. Ortiz, and B. S. Mendoza, Opt. Express **18**, 22119 (2010).
[49] J. Pérez-Huerta, G. P. Ortiz, B. S. Mendoza, and W. L. Mochan, New J. Phys. **15**, 043037 (2013).
[50] W. L. Mochán, B. S. Mendoza, and I. Solís, in *Latin America Optics and Photonics Conference* (Optical Society of America, Washington, 2014), pp. LM2C–2.
[51] B. S. Mendoza and W. L. Mochán, Phys. Rev. B **94**, 195137 (2016).
[52] J. Butet, B. Gallinet, K. Thyagarajan, and O. J. Marti, J. Opt. Soc. Am B **30**, 2970 (2013).
[53] J. Butet, P.-F. cois Brevet, and O. J. F. Martin, ACS Nano **9**, 10545 (2015).
[54] Photonic - A perl package for calculations on photonics and metamaterials v0.010 (2018), https://metacpan.org/pod/Photonic.
[55] J. D. Jackson, *Classical Electrodnamics*, 2nd ed. (Wiley, New York 1975), Sect. 6.7.
[56] B. S. Mendoza and W. L. Mochán, Phys. Rev. B **53**, 4999 (1996).
[57] J. A. Maytorena, B. S. Mendoza, and W. L. Mochán, Phys. Rev. B **57**, 2569 (1998).
[58] P. Guyot-Sionnest and Y. R. Shen, Phys. Rev. B **38**, 7985 (1988).
[59] Y. R. Shen, *The Principles of Nonlinear Optics* (Wiley, Hoboken, NJ, 2003).
[60] R. Haydock, in *Solid State Physics*, Vol. 35 (Academic, New York, 1980), pp. 215–294.
[61] G. P. Ortiz, B. E. Martínez-Zérega, B. S. Mendoza, and W. L. Mochán, Phys. Rev. B **79**, 245132 (2009).
[62] K. Glazebrook and F. Economou, Dr. Dobb's Journal **22** (1997).
[63] S. Ducasse, M. Lanza, and S. Tichelaar, in *Proceedings of the Second International Symposium on Constructing Software Engineering Tools (CoSET 2000)*, Vol. 4 (IEEE, Piscataway, NJ, 2000).
[64] L. Juárez-Reyes, G. P. Ortiz, B. S. Mendoza, and W. L. Mochán (unpublished).
[65] S. Popov, *Susceptibility Tensors for Nonlinear Optics* (Routledge, Abingdon, UK, 2017).
[66] H. U. Yang, J. D'Archangel, M. L. Sundheimer, E. Tucker, G. D. Boreman, and M. B. Raschke, Phys. Rev. B **91**, 235137 (2015).
[67] R. W. Boyd, *Nonlinear Optics* (Elsevier, Amsterdam, 2003).
[68] Much higher susceptibilities have been found in carefully tailored multiple quantum well structures made of noncentrosymmetric materials whose intersubband transitions where coupled to resonances of a plasmonic metasurface. See J. Lee, M. Tymchenko, C. Argyropoulos, P.-Y. Chen, F. Lu, F. Demmerle, G. Boehm, M.-C. Amann, A. Alù, and M. A. Belkin, Nature (London) **511**, 65 (2014).